Fracture characterization through the use of azimuthally sectored attribute volumes

Amanda Thompson and Jamie Rich, Devon Energy Co.*
Mike Ammerman, Ammerman Geophysical

Summary

Azimuthal volumes have often been looked at in conjunction with velocity anisotropy to determine the strike of fractures or maximum stress direction. Due to variations in the directions of fractures, attributes calculated on azimuthal volumes may also provide insight into the strike and dip, location, and spatial variation of the fractures. In particular, attributes highlighting the differences in frequency, time, and amplitude can effectively isolate areas of fractures (Tod et al 2007). If these seismic experiments can detect naturally-occurring fractures in reservoirs then why not use the same principles to detect hydraulically-induced fractures? The techniques discussed in this paper will show how these azimuthally sectored volumes and their attributes can be used to map the hydraulically-induced fractures in the Barnett Shale in the Ft. Worth Basin. Areas of pre-existing hydraulic fractures are typically avoided because of the potential interference with other wells in the area. We demonstrate how prior geologic knowledge of areas of hydraulically-induced fractures will be used in conjunction with the azimuthal volumes in order to effectively map the fractures.

Acquisition and Processing

In April 2009, Devon Energy acquired a wide azimuth 51 km^2 proprietary 3D seismic data over the study area. Overall, the P-wave seismic data are of high quality with frequencies approaching 100 Hz. Table 1 summarizes the acquisition parameters. Offsets equal to or greater than the target depth are acquired.

Table 1: Acquisition parameters used to allow subsequent azimuthal processing

Number of live lines:	30
Number of stations per line:	120
Receiver line interval	660 ft (201 m)
Receiver group spacing	220 ft (67 m)
Shot line interval	880 ft (268 m)
Vibrator array interval	220 ft (67 m)
Patch size	26,180 ft by 25,520 ft (7,980 m by 7,778 m)
Nominal bin size	110 ft by 110 ft (33 m by 33 m)
Number of vibrator sweeps	8
Number of vibrators per array	3
Sweep range	10-110 Hz, 10 s duration, 3 db/octave
Number of geophones per group	6 in a 6 ft (2 m) circle around station

During processing, we first computed the azimuthal velocity variation based on the far-offset azimuthal variation in traveltimes. We then prestack time-migrated the data, and generated four 45^0-wide azimuthally-sectored volumes centered about 0^0 (North), 45^0, 90^0, and 135^0 for further analysis. Figure 1 shows the azimuth (spider diagram) of the midpoints inside representative CMP bins. Since all azimuths are present in the bins this justifies the azimuthal processing. Although Table 1 shows the bin size to be 110 ft by 110 ft (33 m by 33 m), we increased the bin size of the azimuthal sectored volumes to generate 'super gathers' at 220 ft by 220 ft (67 m by 67m) to increase fold. This processing has been implemented in other 3D surveys in the study area, so the fast and slow azimuth directions are known. The fast direction is usually the maximum horizontal stress direction, which for the basin is approximately N45E. There was no need to use multiple azimuths with smaller ranges to first determine the fast and slow directions of the data.

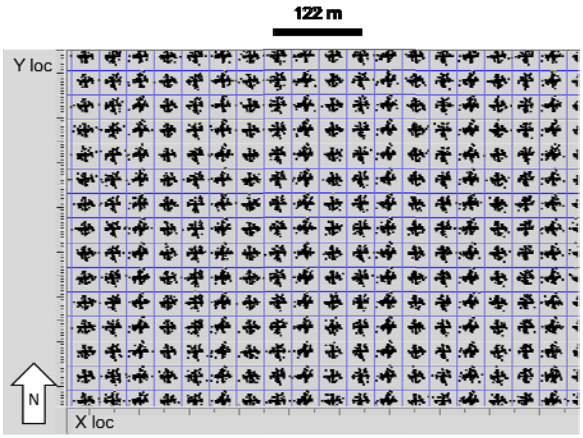

Figure 1. Spider diagram of the azimuthal coverage corresponding to the CMP bins displayed in the red box shown in Figure 4. Note the azimuthal coverage is wide, and close to uniform.

Geologic and Production Data

Within this survey there are several hundred Devon-operated Barnett gas wells, two thirds of which are vertical or directional and the remainder are horizontal wells. In terms of special processes, image logs were run on sixteen wells before April 2009, and two wells after April 2009. Approximately a dozen microseismic experiments were run on another subset of wells before April 2009.

In addition to these specialty log experiments, two production logs have been acquired, four wells have conventional (whole) cores, eight wells have sidewall cores and one well has both conventional and sidewall cores. Completions for vertical wells are within the Upper and Lower Barnett interval and horizontal wells are primarily landed and completed in the Lower Barnett interval; however, there are seven horizontal Upper Barnett completions including one with microseismic.

Azimuthal Attribute Analyses

Typically seismic attributes are run on full-azimuth, full-offset stacked data. In our study a full suite of attributes were run by a third party vendor on each of the four azimuthally sectored volumes. In total 70 attributes that exploit geometric, phase, instantaneous and amplitude differences were calculated on each sectored volume. Horizons were picked on each azimuthally-sectored volume so differences in time between the azimuths could also be reviewed.

The wells are considered to be producing from open, gas-filled fractures, and if orthorhombic symmetry is present (flat layers and one dominant set of vertically-aligned open fractures), then we hypothesize that we should be able to detect open fractures with seismic (Lynn 2004). We also expect the amount of fractures detected to vary by azimuth. Knowledge of fast and slow azimuth directions, velocity anisotropy trends from previous seismic experiments and behavior of the microseismic data will aid in confirming this expectation.

Ellipse Fitting to Azimuthal Volumes

Gretchka and Tsvankin (1998) showed how the NMO velocity in a medium with horizontally transverse symmetry can be fit by an ellipse. Fitting such an ellipse to time delays in azimuthally-sectored data is the standard approach to azimuthal velocity analysis. Our goal here is to exploit the azimuthal variations in waveform, independent of the more common time shifts or amplitude variation with azimuth (AVAz). In order to avoid the overprint of the time-delay anisotropy, the same horizon is interpreted on each of the azimuthally sectored volumes. These horizons are then used to extract a given attribute for each corresponding azimuthally-sectored volume. These attribute values, $A(\theta)$, are then fit to an ellipse using

$$A(\theta) = a\cos^2 + b\cos\theta\sin\theta + c\sin^2\theta \ , \quad (1)$$

by casting equation 1 for each azimuth, θ_j, in matrix form

$$\begin{pmatrix} \cos^2\theta_1 & \cos\theta_1\sin\theta_1 & \sin^2\theta_1 \\ \cos^2\theta_2 & \cos\theta_2\sin\theta_2 & \sin^2\theta_2 \\ \dots & \dots & \dots \\ \cos^2\theta_n & \cos\theta_n\sin\theta_n & \sin^2\theta_n \end{pmatrix} \begin{pmatrix} a \\ b \\ c \end{pmatrix} = \begin{pmatrix} A_1 \\ A_2 \\ \dots \\ A_n \end{pmatrix} . \quad (2)$$

Equation 2 has the form **A=TC**, where **A** are the measured attributes, and **C** are the unknown coefficients, which can be solved using least-squares:

$$\hat{\mathbf{C}} = \left(\mathbf{T^T T}\right)^{-1}\mathbf{T^T A} . \quad (3)$$

In order to find the major and minor axes of the ellipse, we rotate the ellipse by some angle β such that these line up with the local coordinate system. For our problem, the equation of the ellipse can be written as

$$A(\theta) = \lambda_1\cos^2(\theta-\beta) + \lambda_2\sin^2(\theta-\beta) , \quad (4)$$

where λ_1 and λ_2 are the eigenvalues of the matrix formed by the general coefficients

$$\begin{pmatrix} a & b \\ b & c \end{pmatrix} \qquad (5)$$

and where β is the azimuth of the eigenvector associated with the eigenvalue λ_1.The eccentricity, e, (or degree of anisotropy) of the best-fit ellipse is given by

$$e = \sqrt{\left(\frac{\lambda_2^{\,2} - \lambda_1^{\,2}}{\lambda_2^{\,2}} \right)}\ , \qquad (6)$$

while the reliability of the fit is defined as

$$R = \frac{e}{RMSE}. \qquad (7)$$

Where RMSE is the Root mean square error for the best fit ellipse.

After fitting ellipses to all 70 attributes on both the lower Barnett shale and Ordovician Unconformity horizon, the eccentricity, e, as seen in equation 6 and reliability, R, in equation 7 were mapped and compared. Figures 2-5 show the eccentricity and reliability of the wavelet dominant frequency attribute. Barnes (1993) describes the wavelet dominant frequency as a measure of central tendency of the bandwidth. We would expect to see azimuthal variations in the central tendency of the power spectrum due to open fractures.

Notice in Figure 3 that the degree of eccentricity is larger at the top of Ordovician Unconformity than at the top of the lower Barnett shale (Figure 2) indicating a different fracturing regime within the Barnett. Figures 4 and 5 show the reliability calculated at the lower Barnett shale and Ordovician Unconformity. A value of R greater than 6 is considered a statistically significant fit. Anywhere the map is red the fit is valid, which confirms our use of this attribute.

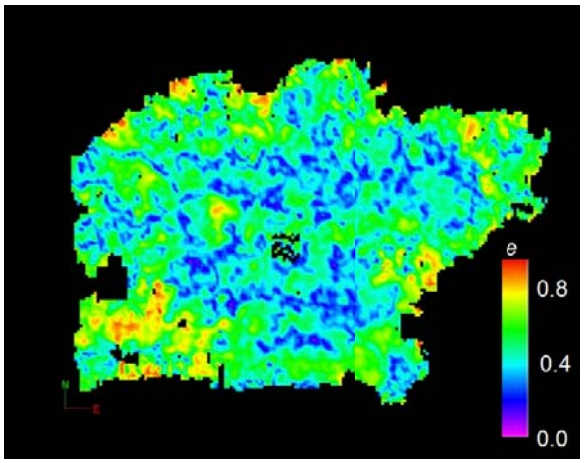

Figure 2. Example of eccentricity calculated on the top of the lower Barnett shale.

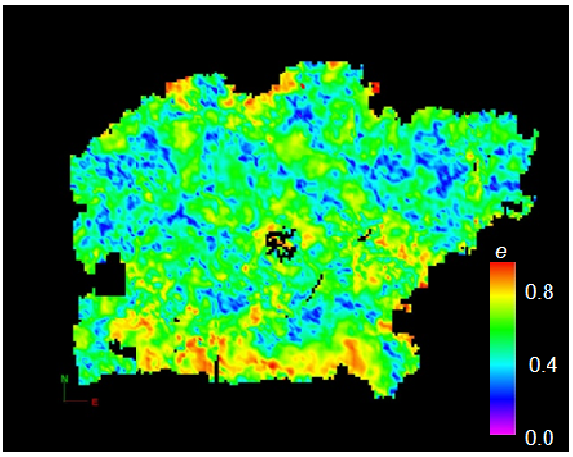

Figure 3. Example of eccentricity calculated on the top of the Ordovician Unconformity

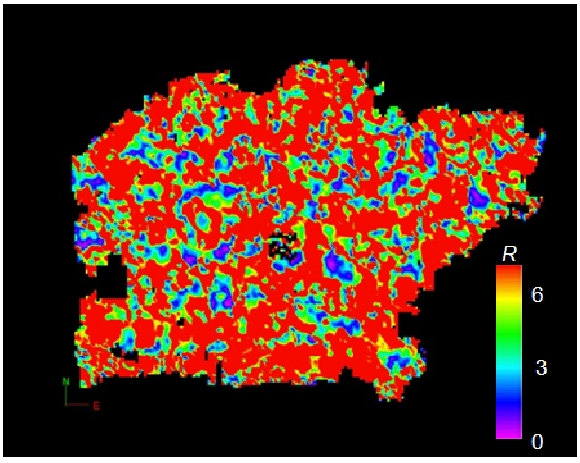

Figure 4. Example of Reliability calculated on the top of the lower Barnett shale.

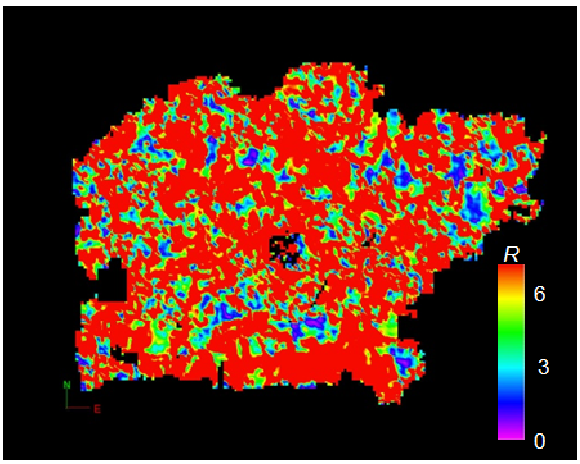

Figure 5. Example of Reliability calculated on the top of the Ordovician Unconformity.

Incorporation of Production Data

Once the seismic data has been fit to an ellipse and the errors in the fit of the ellipse are calculated, the wells were evaluated according to their EUR. These values have been compared to the monthly production rate for April 2009 and January 2010. The data from vertical wells were somewhat simpler to analyze and have been gridded to generate a map. The EUR from the horizontal wells were more challenging and needed to be normalized by lateral length and the number of stages. After normalization, it was possible to scale the horizontal well EUR to be consistent with the vertical well EUR.

Next, the microseismic data, formation imaging logs and core information for the applicable wells were analyzed. For wells with microseismic, the date the well was completed was compared to its first month's production, April 2009 production and January 2010 production. These three values should be an indication of how the well's production has declined by potential closure of the induced fractures. Using the ellipse fitting to the azimuthal volumes we have been able to identify the subset of seismic products that have a good correlation with the production data.

Since there is only one seismic experiment, this is not a traditional time-lapse experiment. Nevertheless, there are several time-lapse components. First, all the wells were logged before fracturing. Second, knowledge of which wells produced well and which produced poorly was used. Third, any potential damage due to induced fractures was seismically mapped. Finally, knowledge of which wells were drilled after the seismic experiment was conducted in 2009, were compared with EUR. Using these data, we anticipated correlation of productivity to attributes insensitive to fracture damage (time-thickness and curvature), and mapped bypassed pay in areas that were thought to have been properly produced. Image logs run on unstimulated wells after April 2009 were looked at toward the end of the seismic analysis to test predictions of where the induced fractures exist. All of the cores were extracted before April 2009 and were used in the same manner as the image logs. The treatment pressures for the wells were used to help determine the induced fracture half-lengths. Treatment pressures, and actual proppant put away into the formation, are recorded by stage for every well and were used to correlate production data and seismic data to the relative values of EUR. These measures can be important indicators of the amount of rock that is hydraulically fractured and how effective the formation is stimulated.

Conclusions

Azimuthal variations in the seismic data can be accentuated through the use of attributes. Mapping the eccentricity and the reliability of the best fit ellipse we are seeing these variations as being indicative of hydraulically induced fractures. Correlation with production data has helped isolate areas of fractures. Future work will quantify the correlation seen visually between the production data and the seismic products. We will be able to generate a variogram that will allow mapping of EUR (or alternatively, induced fracture density) using co-located co-krigging.

Acknowledgements

Grateful thanks to Devon Energy for permission to publish; Prof. Kurt Marfurt, Univ. of Oklahoma, for guidance and insights; Dr. Heloise Lynn, Lynn Inc., for comments and discussions.

References

Barnes, Arthur E., 1993, Instantaneous spectral bandwidth and dominant frequency with applications to seismic reflection data, Geophysics, **58**, 419-428.

Grechka, Vladimir and Ilya Tsvankin, 1998, 3-D description of normal moveout in anisotropic inhomogeneous media. Geophysics, **639**, 1079-1092.

Lynn, Heloise, 2004, The winds of change Anisotropic rocks-their preferred direction of fluid flow and their associated seismic signatures-Part 1, The Leading Edge, 1156-1162.

Tod, Simon, Taylor, Brian, Johnston, Rodney, and Allen, Tony, 2007, Fracture prediction from wide-azimuth land seismic data in SE Algeria: The Leading Edge, 1154-1160.